Biochemistry and Biophysics Reports 46 (2026) 102648

Contents lists available at ScienceDirect

Biochemistry and Biophysics Reports

journal homepage: www.elsevier.com/locate/bbrep

The KLF4-inflammatory pathway is associated with paraquat-induced pulmonary injury and early pro-fibrotic responses

Wei Zhang [a,b,1], Sisi Ye [b,c,1], Jiabao Chen [b,c], Jingjing Cao [b,c], Dongyang Xie [b,c], Xiao Jin [d], Zhefan Xie [b,c,*], Chunlai Fu [a,b,c,**]

[a] First School of Clinical Medicine, Guangdong Medical University, Zhanjiang, Guangdong, 524023, PR China
[b] Department of Emergency Medicine, The Tenth Affiliated Hospital, Southern Medical University (Dongguan People's Hospital), Dongguan, Guangdong, 523039, PR China
[c] Dongguan Key Laboratory of Emergency and Translational Medicine, Dongguan, Guangdong, 523059, PR China
[d] Department of Urolog, The Tenth Affiliated Hospital, Southern Medical University (Dongguan People's Hospital), Dongguan, Guangdong, 523039, PR China

ARTICLE INFO

Keywords:
Paraquat
Pulmonary injury
KLF4
Inflammatory pathway
Early pro-fibrotic responses

ABSTRACT

Paraquat, a highly toxic herbicide, frequently causes acute poisoning, predominantly inducing pulmonary injury and fibrosis with high mortality, and no specific antidote is available. This study aimed to explore its pathogenesis using a paraquat-induced mouse model. Results showed that paraquat caused dose-dependent body weight changes, pulmonary edema, and pathological damage (alveolar structure destruction, inflammatory cell infiltration), with elevated levels of inflammatory factors (IL-6, TNF-α, IL-1β) in BALF and lung tissues. It also induced pulmonary early pro-fibrotic responses, evidenced by increased collagen deposition and upregulated mesenchymal markers (α-SMA, Vimentin, Collagen I). RNA sequencing revealed KLF4 was significantly downregulated, and differentially expressed genes (DEGs) were enriched in inflammatory pathways. KLF4 negatively correlated with core genes (GSK3B, MLH1, PRKACA, VDAC1, WNT7B) in pathways like Wnt signaling pathway. These findings indicated that paraquat-induced pulmonary injury and early pro-fibrotic responses are associated with KLF4 downregulation and inflammatory pathway activation, identifying KLF4 as a potential therapeutic target for clinical intervention.

1. Introduction

Paraquat (1,1′-dimethyl-4,4′-bipyridinium dichloride) is a highly effective, low-cost broad-spectrum herbicide with widespread use in global agriculture [1]. Its high toxicity, however, poses a severe threat to human health. Acute poisoning cases resulting from intentional ingestion, accidental ingestion, or consumption of paraquat are frequent in developing countries, with persistently high incidence in remote rural areas of China [2]. An epidemiological study covering 2016 to 2022 confirmed pesticide poisoning as the most prevalent acute poisoning type in China, accounting for 30.4% of all acute poisoning cases [3]. Among these pesticide-related incidents, the mortality rate of paraquat poisoning ranking third among various types of pesticide poisoning (7.05%) [3]. In addition, paraquat enters the body via respiratory, gastrointestinal, or dermal exposure, with the lung as its primary target [4]. Affected patients may exhibit symptoms like vomiting, diarrhea, and oral ulcers; severe cases can progress to acute pulmonary injury, potentially culminating in death [5]. Currently, no specific antidote exists for paraquat poisoning. Thus, in-depth clarification of the pathogenesis underlying paraquat-induced pulmonary injury and development of effective interventions carried substantial clinical and public health significance.

Currently, the mechanism of paraquat-induced pulmonary injury remains incompletely elucidated, with its pathogenesis primarily linked to factors including the molecular structure of paraquat, redox reactions in organisms, and inflammatory responses [6,7]. Owing to the high

* Corresponding author. Department of Emergency Medicine, The Tenth Affiliated Hospital, Southern Medical University (Dongguan People's Hospital), Dongguan, Guangdong, 523059, PR China.
** Corresponding author. Department of Emergency Medicine, The Tenth Affiliated Hospital, Southern Medical University (Dongguan People's Hospital), Dongguan, 523039, Guangdong, PR China.
E-mail addresses: 642464021@qq.com (Z. Xie), fcldgsrmyy@163.com (C. Fu).
[1] These authors contributed equally to this work.

https://doi.org/10.1016/j.bbrep.2026.102648
Received 14 October 2025; Received in revised form 15 May 2026; Accepted 22 May 2026

abundance of polyamine transporters in lung tissues, paraquat, structurally homologous to endogenous polyamines, was actively taken up and accumulated in the lungs at concentrations 6-10 times those in plasma, thereby inducing pulmonary injury and subsequent fibrosis [8,9]. Additionally, paraquat exhibited strong oxidizing and corrosive properties. Upon entering the lungs, it accumulated in alveolar epithelial cells, where it induced excessive production of reactive oxygen species. This triggered lipid peroxidation, DNA damage, and mitochondrial dysfunction [6]. Concurrently, paraquat activated the NF-κB pathway, promoting the release of pro-inflammatory cytokines such as TNF-α and IL-1β, and inducing NLRP3 inflammasome assembly, which collectively initiated a robust inflammatory response [10]. Clinical study demonstrated that patients with moderate to severe paraquat poisoning frequently developed typical pulmonary fibrosis in the advanced stages, often accompanied by dyspnea or even respiratory failure. This represented one of the primary causes of death in such patients [11]. The development of pulmonary fibrosis was closely associated with abnormal expression of molecules including α-SMA, Vimentin, CollagenI, and TGF-β1 [12]. It should be noted that early pro-fibrotic responses, the reversible initial cellular and molecular events preceding overt pulmonary fibrosis, are the critical preliminary stage of toxicant-induced pulmonary fibrosis development [13]. Due to the limited modeling time, we only observed early pro-fibrotic responses without reaching the stage of pulmonary fibrosis. The present study aimed to explore potential regulatory targets involved in paraquat-induced pulmonary injury and the subsequent development of early pro-fibrotic responses.

Bioinformatics analysis, an interdisciplinary discipline integrating computational science, statistics, and mathematics, explores biological issues through the acquisition, storage, analysis, and visualization of biological data to reveal their underlying mechanisms. It has become a key tool in modern biomedical research for elucidating the pathogenesis of complex diseases and identifying biomarkers [14,15]. Previous studies showed that Krüppel-like factor 4 (KLF4) played a protective role in various cancers through multiple pathways, such as anti-inflammation, epithelial barrier protection, resistance to oxidative stress, and regulation of fibrosis [16]. Additionally, KLF4 was confirmed to be involved in the resolution of inflammation during lung injury [17,18]. Building on this, the present study, in combination with bioinformatics analysis, intended to clarify the role and mechanism of KLF4 in lung injury.

In this study, based on a paraquat-induced in vivo model, it was found that mouse lung tissues exhibited typical pathological changes of pulmonary injury and even early pro-fibrotic responses, such as alveolar structure destruction, inflammatory cell infiltration, and collagen fiber deposition. Meanwhile, the expression levels of pro-inflammatory factors and fibrosis-related indicators in lung tissues were significantly increased. Further analysis via RNA sequencing and differentially expressed genes (DEGs) analysis showed that KLF4 was significantly downregulated; combined with the results of Kyoto Encyclopedia of Genes and Genomes (KEGG) pathway analysis, it was observed that the target genes of KLF4 were enriched in inflammatory signaling pathways. Collectively, the KLF4-inflammation pathway was a potential regulatory target associated with paraquat-induced pulmonary injury, worthy of further mechanistic exploration.

2. Materials and methods

2.1. Animals

This study was carried out in compliance with the ARRIVE guidelines (https://arriveguidelines.org). The animal protocols were reviewed and approved by the Laboratory Animal Welfare and Ethics Committee of Dongguan People's Hospital (Approval No.: IACUC-AWEC-202409500). Male C57BL/6 mice (6-8 weeks old, 20-24 g) were obtained from the Guangdong Medical Laboratory Animal Center. All mice were housed in a specific pathogen-free (SPF) conditions with controlled temperature (22 ± 2 °C), humidity (50 ± 5%), and a 12 h light/12 h dark cycle. A total of 9 mice were assigned to each experimental group, with a maximum of 5 mice per cage. Paraquat (HY–B0864A) was purchased from Med Chem Express (MCE, Shanghai, China) and dissolved in saline. Mice in the paraquat groups received intraperitoneal injections of paraquat at 10, 20, or 30 mg/kg, respectively, and were observed for 2 days. This route was selected based on prior studies demonstrating stable pulmonary injury model establishment, enabling uniform systemic paraquat distribution to mimic severe clinical poisoning where paraquat enters circulation via mucosal absorption [19,20]. The control group received an equal volume of saline. Specifically, the initial body weight of each mouse was recorded, with reweighing performed at 48 h post-administration. At 48 h after treatment, all mice were euthanized humanely. Subsequently, mouse bronchoalveolar lavage fluid (BALF) was collected via tracheal cannulation, and lung tissues were harvested for systematic and rational lobe allocation to complete multiple parallel experiments (no mice or samples were excluded in all groups, $n = 9$ per group): the left lung lobes of 4 randomly selected mice per group were used solely for the measurement of lung wet-to-dry (W/D) weight ratio; the left lung lobes of the remaining 5 mice were fixed in 4% paraformaldehyde for pathological detection (HE staining, Masson's trichrome staining, IHC), as the larger left lung structure can more clearly reflect pulmonary injury and fibrotic characteristics; the right lung lobes of all 9 mice were divided and snap-frozen in liquid nitrogen: most were used for WB analyses, while the right lung lobes of 4 mice in the 30 mg/kg paraquat-treated group were specifically selected for bioinformatics analyses (RNA sequencing) due to the most prominent inflammatory responses in this group. Body weight was measured for all 9 mice before and after paraquat exposure as a non-invasive index.

For measurement of the lung W/D weight ratio: the left lung tissues of the 4 assigned mice were harvested, weighed immediately to obtain the wet weight, then dried in a 60 °C metal bath for 48 h until the weight was stable. The dry weight was then measured, and the W/D ratio was calculated. All animal procedures and data reporting in this manuscript fully comply with the ARRIVE 2.0 guidelines to ensure transparency, reproducibility, and scientific rigor.

2.2. Hematoxylin-eosin (HE) and Masson's trichrome staining assays

For the HE staining assay, lung sections were dewaxed in xylene and rehydrated through graded alcohols. After hematoxylin staining and rinsing, the sections were differentiated in 1% hydrochloric acid alcohol and subsequently blued under running water. Following eosin staining, the sections were dehydrated through graded alcohols, cleared in xylene, and mounted with neutral gum. For Masson's trichrome staining, after hematoxylin staining, the lung sections were stained with ponceau-fuchsin (to stain muscle fibers red), treated with 1% phosphomolybdic acid, and then stained with aniline blue (to stain collagen fibers blue). After dehydration through graded alcohols and clearing in xylene, the sections were mounted with neutral balsam.

Tissue structures were examined microscopically. Pulmonary injury was recorded and graded 0 - 4 based on the following criteria: 0 (No damage); 1 (Slight, diffuse neutrophilic damage in alveolar walls without wall thickening or hemorrhage; alveolar space congestion <25%); 2 (Diffuse mononuclear and neutrophilic damage in alveolar walls with mild thickening; ≥5 erythrocytes in 1–5 alveoli; alveolar congestion 25–30%); 3 (Alveolar wall thickening (2–3x normal); ≥5 erythrocytes in 5–10 alveoli; alveolar congestion 30–50%); 4 (Alveolar wall thickening with ≥50% lung consolidation; ≥5 erythrocytes in >10 alveoli; alveolar congestion >60%) [21]. The proportion of collagen fiber area was quantified using ImageJ software.

2.3. Enzyme-linked immunosorbent assay (ELISA)

IL-1β (1110122), IL-6 (1210602), and TNF-α (1217202) Precoated

ELISA Kits, purchased from Dakewe Biotechnology (Beijing, China), were used to quantitatively measure the inflammatory factors according to the manufacturer's protocols.

2.4. Western blot (WB) assay

Total proteins were extracted from the lungs of mice using RIPA buffer (Labgic Technology, Beijing, China), and their concentrations were determined with a Bicinchoninic Acid (BCA) Protein Assay Kit (NCM Biotechnology, Suzhou, China). The proteins were then separated by 10% SDS-PAGE gels and subsequently transferred to polyvinylidene fluoride (PVDF) membranes (Millipore, Billerica, Massachusetts, USA). After blocking the membranes with 3% bovine serum albumin (BSA) (Labgic Technology, Beijing, China) for 60 min, they were incubated with primary antibodies at 4 °C overnight. These primary antibodies, all sourced from Proteintech (Chicago, USA), included TNF-alpha (TNF-α, 1:2000, 60291-1-Ig), IL-1 beta (IL-1β, 1:3000, 10842-1-AP), alpha smooth muscle actin (α-SMA, 1:4000, 14395-1-AP), Vimentin (1:20000, 10366-1-AP), Collagen Type I (Collagen I, 1:2000, 14695-1-AP), and beta-actin (β-actin, 1:20000, 66009-1-Ig). Subsequently, the membranes were incubated with the secondary antibody (1:5000, Bioworld, Nanjing, China) at room temperature for 1 h. Using β-actin as the internal control, target proteins were visualized with a chemiluminescence kit (NCM Biotechnology, Suzhou, China), and membrane intensity was analyzed using ImageJ software.

2.5. Immunohistochemistry (IHC) staining assay

Mouse lung tissues were first paraffin-embedded and subsequently deparaffinized in xylene. The tissue sections were treated with 3% hydrogen peroxide-methanol to quench endogenous peroxidase activity, followed by dehydration in graded alcohols and antigen retrieval in sodium citrate buffer. After blocking with 3% BSA for 30 min, the sections were incubated overnight at 4 °C with anti-KLF4 primary antibody (1:200, Proteintech, Chicago, USA), then with the corresponding secondary antibody (Servicebio, Wuhan, China) and visualized using DAB (3,3′-diaminobenzidine tetrahydrochloride; Servicebio, Wuhan, China). After color development, the sections were rinsed with running water, counterstained with hematoxylin, mounted on slides with DPX (dibutyl phthalate xylene), and examined microscopically. The staining intensity was analyzed using ImageJ software.

2.6. Bioinformatics analyses

Based on findings from HE staining and ELISA assays, the 30 mg/kg paraquat-treated group exhibited the most prominent inflammatory responses in mice compared to the control group. Consequently, the study further collected 4 mouse lung tissues from each of the control group and the 30 mg/kg paraquat-treated group for bioinformatics analyses.

Prior to bioinformatics analyses, strict quality control (QC) and data preprocessing were performed to ensure data reliability. Raw sequencing data were first evaluated using FastQC software, including key indicators: per base sequence quality (average Phred score >30), sequence length distribution, GC content, adapter content, and over-represented sequences. Low-quality reads (Phred score <20) and adapter sequences were removed using Trimmomatic software to obtain clean reads. Clean reads were aligned to the mouse reference genome (mm10) using HISAT2 with an alignment rate >90%. Gene expression levels were quantified using FeatureCounts, including raw reads count and normalized FPKM values (to eliminate the interference of sequencing depth and gene length). For DEG analysis, the DESeq2 package was used for data normalization (median of ratios method) and dispersion estimation (local dispersion model); no batch effects were observed among samples, so no batch correction was performed.

2.6.1. Determination of differentially expressed genes (DEGs)

DEGs between paraquat-treated and control samples were identified using the DESeq2 package in R, with data normalization performed via the median of ratios method embedded in the package and dispersion estimated using the local dispersion model to improve identification accuracy. DEGs were defined by the thresholds of $|\log2 \text{ Fold Change (log2FC)}| > 1$ and FDR-adjusted p-value (padj) < 0.05, where FDR correction was implemented to control false positive results. Volcano plots were subsequently generated with the ggplot2 R package to visualize the distribution of DEGs, including upregulated and downregulated subsets.

2.6.2. Functional enrichment analysis

Kyoto Encyclopedia of Genes and Genomes (KEGG) pathway enrichment analysis was performed using clusterProfiler R package for DEGs and key target genes identified in Sections 2.6.1 and 2.6.3, respectively. KEGG pathways with an FDR-adjusted p-value (padj) < 0.05 were regarded as statistically significant. Bubble plots were generated with the ggplot2 R package to visualize the enrichment results.

2.6.3. Systematic screening and validation of key target genes

Drawing on Sections 2.6.1, 2.6.2, and published literature, KLF4 was initially identified as a key gene linked to paraquat-induced pulmonary injury. Potential KLF4 target genes were first retrieved from the GeneCards databases (human reference) based on the presence of KLF4-binding CACCC motifs) within promoter regions. To match our mouse in vivo model, human candidate genes were converted to their mouse orthologs using the NCBI HomoloGene database. The screening criteria included: ① ≥ 10 CACCC sequences within promoter regions; ② negative expression correlation with KLF4 (correlation coefficient $r < -0.3$ with p-value <0.01); ③ documented involvement in inflammatory processes validated by published studies.

Subsequently, KEGG pathway enrichment analysis was performed on these conserved mouse orthologs to assess their enrichment in oxidative stress, inflammatory response, and apoptosis, which represent core mechanisms underlying paraquat-induced pulmonary injury. Expression levels of KLF4 and its candidate target genes were compared between groups using box plots and two-tailed Student's t-test (stat_compare_means function in the ggpubr package). Linear regression were employed to analyze expression correlations between KLF4 and its target genes. FDR adjustment was used for all p-values to control for false positives.

2.7. Statistical analysis

Quantitative data are expressed as mean ± standard deviation (SD), with biological replicates and technical replicates clearly defined as follows: (1) Biological replicates: Each experimental group contained 9 mice (biological replicates), with tissue allocation specified in Section 2.1; (2) Technical replicates: HE staining, ELISA, WB, Masson's trichrome staining and IHC analysis were performed in triplicate (three technical replicates) to ensure data reliability. Differences between two groups were analyzed using the two-tailed Student's t-test. For multiple group comparisons, one-way analysis of variance (ANOVA) was used followed by Tukey's multiple comparison test for pairwise comparisons. All statistical analyses were performed via via the R program (version 4.2.2) and SPSS software (version 25.0), with a p-value <0.05 deemed statistically significant.

3. Results

3.1. Paraquat induced pulmonary injury in mice

Paraquat was used to conduct a pulmonary injury model. Compared with the control group, the mice showed greater changes in body weight

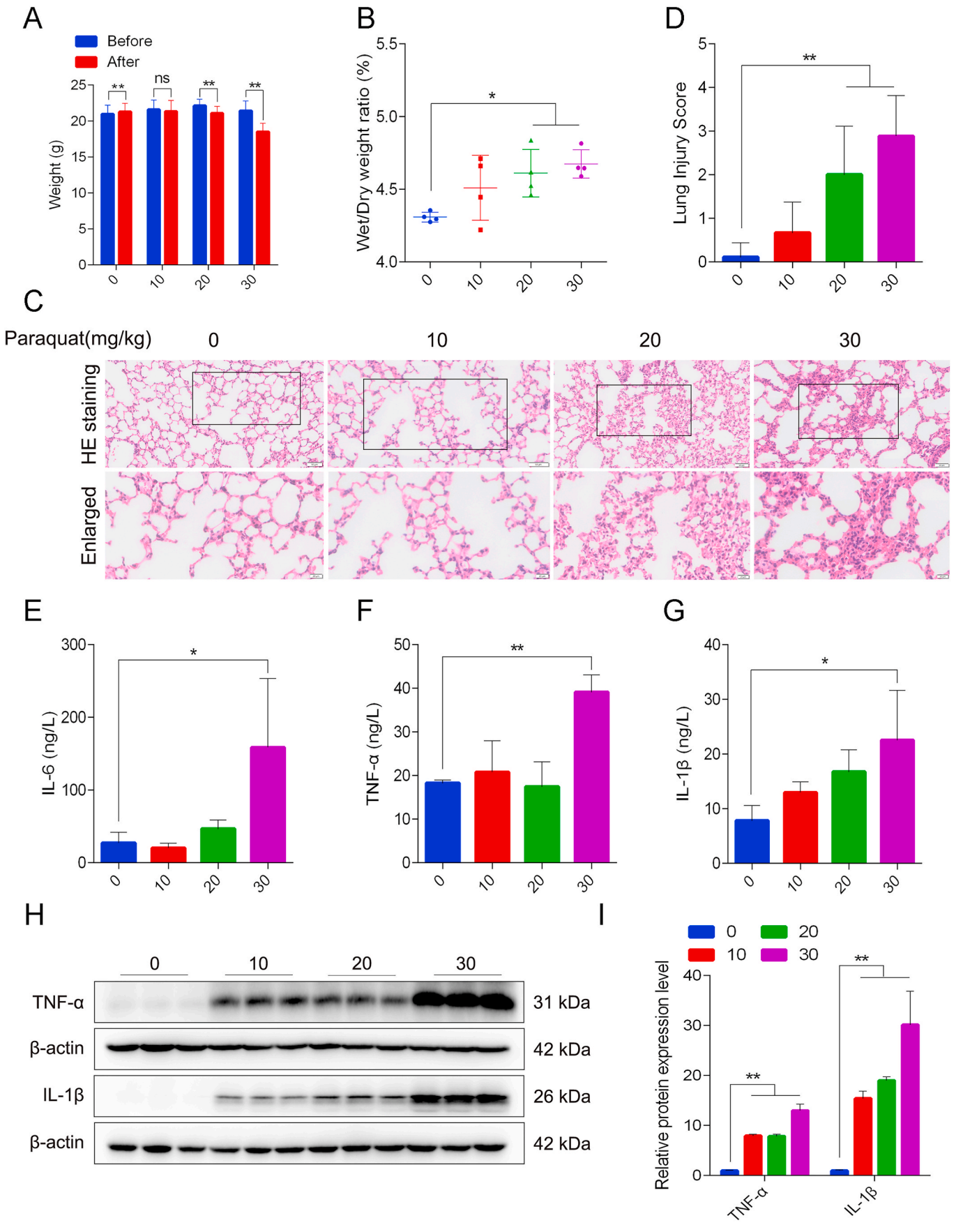

(caption on next page)

Fig. 1. Paraquat induced pulmonary injury in mice. (A) The changes in body weight of mice 48 h after paraquat exposure. ($n = 9$, *t*-test, $^{**}P < 0.01$) (B) The wet/dry ratio of lung of mice 48 h after paraquat exposure. ($n = 4$, one-way ANOVA, $^{*}P < 0.05$). (C-D) Representative micrographs for Hematoxylin-Eosin (HE) staining in mice lung tissues. Original magnification ×10 and ×40. Bar = 50 μm and 20 μm. And bar graphs of pathological injury scores from HE staining results of mouse lung tissues. ($n = 5$, one-way ANOVA, $^{**}P < 0.01$) (E-G) ELISA was performed to analyze IL-6, IL-1β and TNF-α in the bronchoalveolar lavage fluid (BALF) of mice treated with paraquat at doses of 0, 10, 20, or 30 mg/kg ($n = 9$, one-way ANOVA, $^{*}P < 0.05$. $^{**}P < 0.01$) (H–I) Western blotting (WB) was performed to analyze IL-1β and TNF-α in mouse lung tissues treated with paraquat at doses of 0, 10, 20, or 30 mg/kg. And quantitative analysis for protein bands of IL-1β and TNF-α. ($n = 5$, one-way ANOVA, $^{*}P < 0.05$. $^{**}P < 0.01$).

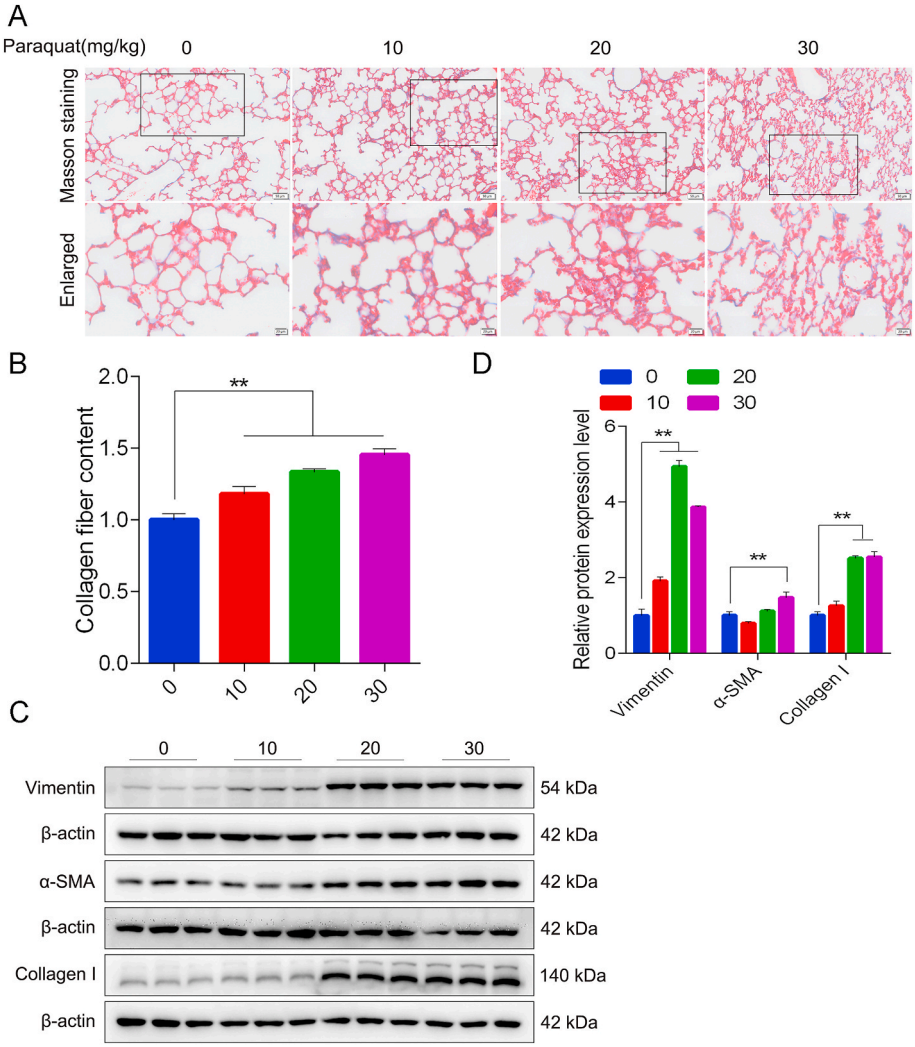

Fig. 2. Paraquat exposure induced pulmonary early pro-fibrotic responses in mice. (A-B) Representative micrographs for Masson's trichrome staining in mice lung tissues. Original magnification ×10 and ×40. Bar = 50 μm and 20 μm. And quantitative analysis for the area of blue collagen fibers. ($n = 5$, one-way ANOVA, $^{**}P < 0.01$) (C-D) Western blotting (WB) was performed to analyze Vimentin, α-SMA, and Collagen 1 in mouse lung tissues treated with paraquat at doses of 0, 10, 20, or 30 mg/kg. And quantitative analysis for protein bands of Vimentin, α-SMA, and Collagen I. ($n = 5$, one-way ANOVA, $^{*}P < 0.05$. $^{**}P < 0.01$).

before and after paraquat administration. The higher the concentration of paraquat, the greater the change in body weight (Fig. 1A). The W/D ratio of lung in the model group was also higher than that in the control group, suggesting that paraquat induced pulmonary edema in mice (Fig. 1B). HE staining presented varying degrees of pathological damage in the model group. Specifically, intact alveolar structure and slight inflammatory exudation was observed in the lung tissues of mice exposed to paraquat at 10 mg/kg, without alveolar septal thickening or alveolar edema. When exposed to paraquat at 20 mg/kg, the lung tissues exhibited a large number of inflammatory cell infiltration, alveolar septal thickening, and alveolar structural destruction. These symptoms exacerbated as the exposure concentration increased (at 30 mg/kg) (Fig. 1C). Furthermore, we scored the degree of pulmonary injury based on the results of HE staining, whose results also confirmed that the higher the concentration of paraquat exposure, the higher the pulmonary injury score (Fig. 1D).

ELISA assay and WB assay were performed to detect changes in the expression levels of inflammatory factors in mice. The results showed that paraquat promoted the expression of IL-6, TNF-α and IL-1β in BALF (Fig. 1E–G), as well as the protein expression levels of IL-1β and TNF-α in lung tissue (Fig. 1H–I). These results suggest that paraquat induced pulmonary injury in mice.

3.2. Pulmonary early pro-fibrotic responses occurred following paraquat exposure

Masson's trichrome staining and WB assay were used to assess the extent of pulmonary early pro-fibrotic responses in the in vivo model.

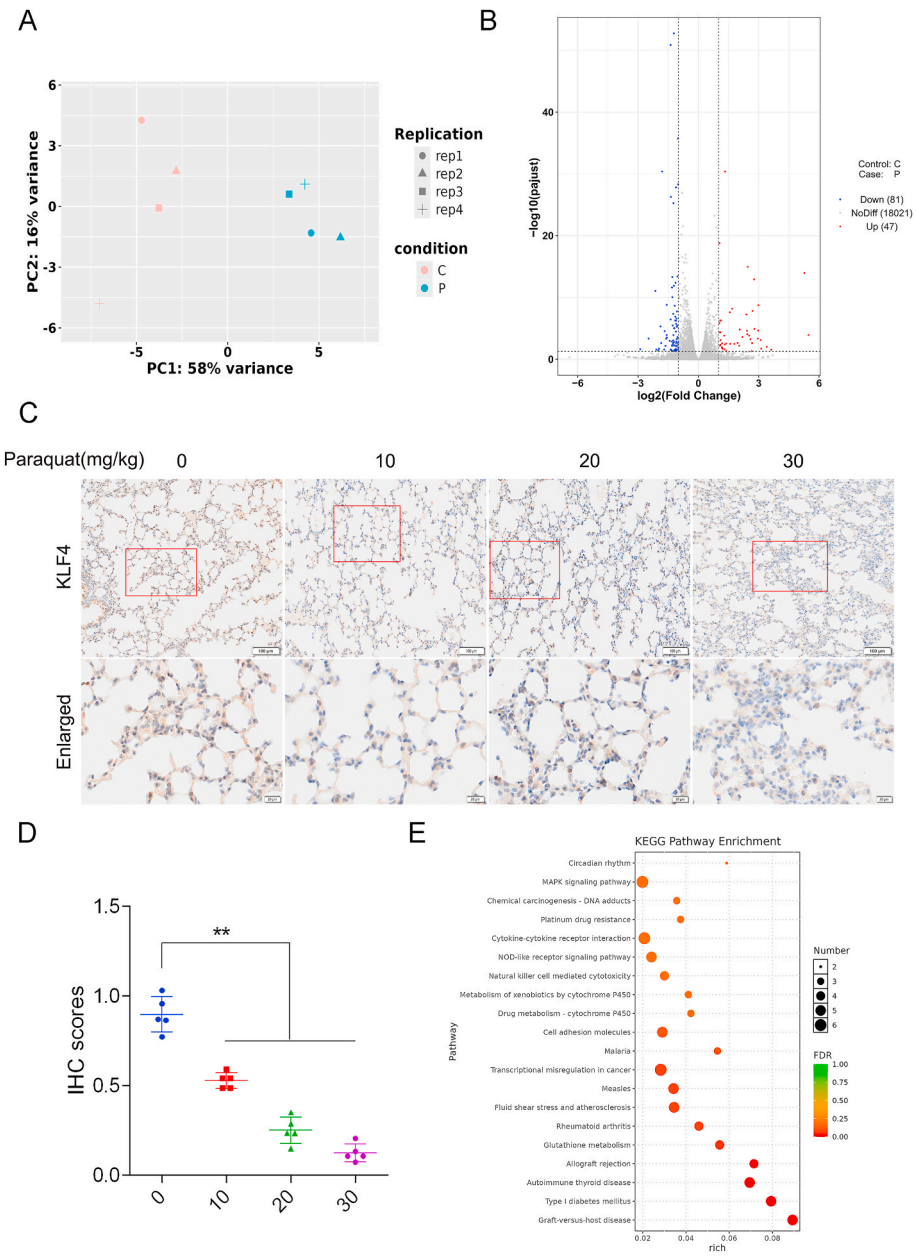

Fig. 3. Paraquat exposure dysregulated gene expression and related signaling pathways in mouse lung tissues. (A) Principal component analysis (PCA) plot with colored points for different groups; closer points meant greater similarity in sample species composition. ($n = 4$) (B) Volcano plot of differentially expressed genes (DEGs), with red denoting upregulation and blue denoting downregulation. ($n = 4$, $|\log2FC| > 1$, FDR-adjusted P-value <0.05) (C-D) Representative immunohistochemistry (IHC) for KLF4 in mouse lung tissues among the control group and paraquat-treating group. Original magnification ×10 and ×40. Bar = 100 μm and 20 μm. And quantitative analysis for KLF4 positive area in mouse lung tissues. ($n = 5$, one-way ANOVA, $^{**}P < 0.01$) (E) KEGG enrichment pathway of differential expressed genes (DEGs), and the bubble plots visualizing the results of enrichment analysis. ($n = 4$, FDR-adjusted P-value <0.05).

Relative to controls, paraquat-treated groups exhibited the deposition of blue fibrous strand to varying degrees; higher paraquat concentrations correlated with more such strands in lung (Fig. 2A–B). This indicated the proliferation and deposition of collagen fiber caused by paraquat in mouse lungs. Epithelial-mesenchymal transition (EMT) of alveolar epithelial cells has been verified to be involved in the development of pulmonary fibrosis. We demonstrated that paraquat increased the levels of mesenchymal markers α-SMA, Vimentin, and Collagen I in lung tissues. These results collectively indicated that paraquat can induce pulmonary early pro-fibrotic responses in mice (Figure C-D).

3.3. *Paraquat dysregulated genes and related pathways in lung tissues of mice*

To validate our acute paraquat poisoning model in mice for validity and consistency, principal component analysis (PCA) was first performed. Samples from paraquat-treated and control groups showed marked separation in the principal component space, indicating intergroup differences. Moreover, tight intra-group clustering reflected good consistency within each group (Fig. 3A). Differentially gene expression analysis was carried out on paraquat-treated and control groups with the aim of identifying gene expression patterns in mice with pulmonary injury. This yielded 128 DEGs: 81 downregulated and 47 upregulated (Supplementary Table 1). Notably, among the

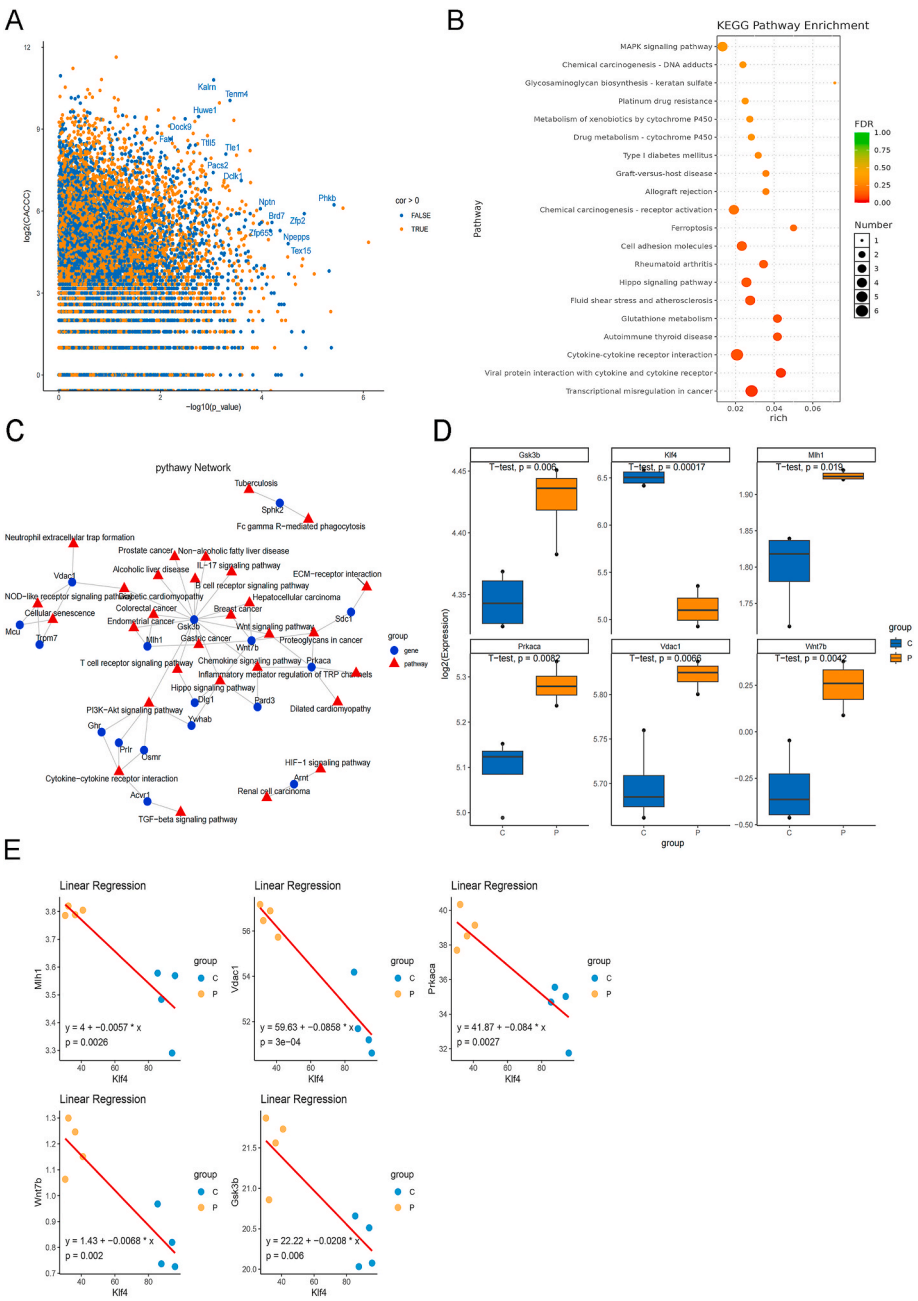

Fig. 4. Paraquat-induced KLF4 downregulation correlated with inflammatory pathway activation in pulmonary injury. (A) Scatter plot of the correlation between KLF4 and target genes with more than ten CACCC sequences. ($n = 4$) (B) KEGG pathway enrichment of KLF4 target genes and bubble plots illustrating the enrichment analysis results. ($n = 4$, FDR-adjusted P-value <0.05) (C) Core gene networks of inflammation-related signaling pathways. (D) Box plots showed the expression levels of KLF4 and core genes of inflammation-related signaling pathways in the control group and the paraquat-treated group. ($n = 4$, two-tailed Student's t-test, $P < 0.05$, $P < 0.01$) (E) Linear regression plot of the expression levels between KLF4 and core gene of inflammation pathways, such as GSK3B, MLH1, PRKACA, VDAC1 and WNT7B. ($n = 4$, linear regression analysis, $P < 0.05$).

downregulated genes, KLF4 and PDE4B exhibited significantly decreased expression (Supplementary Table 1, Fig. 3B). Additionally, versus controls, paraquat reduced KLF4 expression in lung tissues, confirming its involvement in paraquat-induced pulmonary injury (Fig. 3C–D).

Gene functions and biological signaling pathways associated with the above screened DEGs were further identified by KEGG pathway analysis. According to Fig. 3E, DEGs were dominant enriched in MAPK signaling pathway, cytokine-cytokine receptor interaction, cell adhesion molecules, transcriptional misregulation in cancer, which preliminarily suggest the potential association of these DEGs with the development of pulmonary inflammation (Fig. 3E).

3.4. Paraquat-induced KLF4 downregulation correlated with inflammatory pathway activation in pulmonary injury

As a member of the KLFs family, KLF4 is known to play a pivotal role in the pathogenesis of diverse inflammatory diseases [17,18]. The CACCC motif represents a highly conserved KLF4-binding sequence across human and mouse genomes [22,23]. To identify downstream targets in our mouse model, we first retrieved candidate genes containing KLF4-binding CACCC motifs from the GeneCards database (human) and then converted them to mouse orthologs using NCBI HomoloGene. Candidate genes with conserved promoter motifs, negative expression correlation with KLF4, and documented roles in mouse

pulmonary inflammation/fibrosis were selected for further analysis (Fig. 4A). KEGG pathway analysis revealed that these KLF4-related mouse orthologs were significantly enriched in MAPK signaling pathway, chemical carcinogenesis-receptor activation, cell adhesion molecules, Hippo signaling pathway, cytokine-cytokine receptor interaction, transcriptional misregulation in cancer, suggesting KLF4 was potentially associated with the regulation of these pathways in pulmonary inflammatory responses (Fig. 4B–C).

Thereafter, an analysis was conducted on the relationship between KLF4 and core genes within inflammation-related signaling pathways. The results of the boxplot analysis demonstrated that KLF4 expression was significantly lower in the paraquat-treated group, while expression of its predicted target genes (GSK3B, MLH1, PRKACA, VDAC1, WNT7B) was markedly higher (Fig. 4D). To quantify the association between KLF4 and these target genes, Pearson linear correlation analysis was performed (sample size n = 4). The results revealed negative correlation between KLF4 and each of these targeted genes (Fig. 4E). These findings indicated that paraquat exposure was associated with KLF4 downregulation, with all correlations meeting the pre-specified criteria of an uncorrected p-value <0.01 and a correlation coefficient $r < -0.3$: (1) KLF4 vs. MLH1: $r = -0.8956$, $p = 0.0026$, 95% CI [−0.9811, −0.5176]; (2) KLF4 vs. VDAC1: $r = -0.9506$, $p = 0.0003$, 95% CI [−0.9913, −0.7449]; (3) KLF4 vs. PRKACA: $r = -0.8952$, $p = 0.0027$, 95% CI [−0.9810, −0.5161]; (4) KLF4 vs. WNT7B: $r = -0.9042$, $p = 0.0020$, 95% CI [−0.9827, −0.5499]; (5) KLF4 vs. GSK3B: $r = -0.8609$, $p = 0.0060$, 95% CI [−0.9744, −0.3972]. These findings collectively indicated that paraquat exposure was correlated with the loss of potential transcriptional suppression of downstream inflammation-associated genes and subsequent inflammatory pathway activation in pulmonary injury.

4. Discussion

Paraquat, a widely utilized herbicide in China's agricultural sector, effectively controls weeds to reduce pest infestations, thereby enhancing crop productivity. However, acute paraquat poisoning remains prevalent, predominantly resulting from accidental exposure or intentional ingestion, with a mortality rate ranking third among all types of pesticide poisoning [3]. Notably, the unique polyamine structure of lung tissue renders it the primary target for paraquat accumulation in the human body, triggering irreversible pulmonary damage such as acute lung injury and pulmonary fibrosis [8,9]. Clinically, paraquat poisoning exhibited multisystem involvement: its toxic components directly impaired mitochondrial function, leading to hepatocyte and renal cell necrosis, which manifested as elevated transaminases and acute renal failure [24]. It disrupted the blood-brain barrier via redox reactions and stress effects, inducing cerebral edema and neurodegenerative lesions [5]. Additionally, it directly eroded the gastrointestinal mucosa, causing hemorrhage and ulceration [25]. To date, no specific antidote for paraquat poisoning has been identified in domestic and international research. Consequently, extensive efforts are underway to develop novel therapeutic agents and intervention strategies based on its toxic mechanisms, aiming to improve patient survival rates and prevent irreversible organic damage or fatal outcomes.

Rationale for intraperitoneal injection. The intraperitoneal route was selected for three reasons. Firstly, prior studies [19,20] validated that the use of intraperitoneal injection established stable paraquat-induced pulmonary injury models, with results comparable to clinical severe poisoning (systemic drug distribution). Secondly, this study focused on the role of KLF4 in inflammatory pathways, requiring uniform pulmonary drug distribution, while intratracheal or intranasal routes may cause uneven local exposure. Thirdly, severe clinical paraquat poisoning involved drug entry into circulation via mucosal absorption, and intraperitoneal injection mimicked this systemic distribution.

This study established a paraquat-induced poisoning model in mice to observe pathological changes of pulmonary injury and early pro-fibrotic responses. Results demonstrated that paraquat exposure induced significant toxic reactions and lung pathological changes in mice. Mice in the paraquat exposure group exhibited toxic symptoms including poor mental state, reduced appetite, dull and fluffy hair, and delayed response, which aggravated with increasing paraquat concentration. This was consistent with previous findings [26] showing dose-dependent behavioral changes (decreased activity, reduced food intake, and rough hair) in experimental animals after paraquat poisoning, possibly associated with paraquat-induced impairments in systemic metabolism and tissue function. Additionally, the lung W/D weight ratio was higher in the paraquat group than in the control group, with an increasing trend (non-significant) alongside elevated paraquat concentrations. This may be attributed to the subacute stage at 48 h post-modeling. As reported [27], early fat embolism syndrome (12-24 h) caused alveolar capillary barrier disruption and increased vascular permeability, leading to pulmonary edema and elevated W/D ratio. In contrast, fibroblast activation and collagen deposition during the fibrotic stage (>48 h) may reduce the W/D ratio. Our 48 h results aligned with this time-dependent pattern. HE staining revealed intact lung structure without exudation or inflammatory infiltration in the control group, whereas the paraquat exposure group showed dose-dependent pathological changes, including alveolar collapse, red blood cell exudation, interstitial edema, and neutrophil infiltration. Consistent with prior studies [28] demonstrating dose-dependent pulmonary injury (alveolar destruction, inflammatory infiltration, interstitial edema) after paraquat exposure, these findings suggested early inflammatory activation as a core mechanism of paraquat-induced pulmonary injury. Masson staining showed blue collagen fiber deposition in paraquat-exposed lung tissues, with denser deposition at higher concentrations, confirming early pro-fibrotic responses. Mechanistically, paraquat directly induced alveolar epithelial cell apoptosis and disrupted alveolar barriers [29]. Paraquat exposure activated TGF-β to promote fibroblast-to-myofibroblast differentiation and increase type I/III collagen secretion [30]. These results were consistent with our observations. ELISA and WB assays showed elevated levels of IL-6, TNF-α, and IL-1β in alveolar lavage fluid and lung tissues of paraquat-exposed mice, with significance at 30 mg/kg. As reported [31], paraquat poisoning increased pro-inflammatory factors (IL-6) to aggravate alveolar injury via inflammatory cascades. WB analysis of fibrotic markers showed upregulated α-SMA (myofibroblast marker), Vimentin (mesenchymal cell marker), and Collagen1 in paraquat groups, confirming early pro-fibrotic responses. Consistent with prior study [32], α-SMA expression positively correlated with fibrosis severity, reflecting myofibroblast activation. Elevated Vimentin indicated enhanced extracellular matrix (ECM) remodeling [33]. Notably, no significant dose-effect relationship between paraquat concentration and fibrotic proteins was observed within 48 h, likely due to the chronic nature of fibrosis requiring longer observation periods for detectable protein metabolic changes. In conclusion, paraquat poisoning induced pulmonary injury and early pro-fibrotic responses in mice via inflammatory responses, activation of fibrotic signaling pathways, and collagen deposition, consistent with literature reports [34]. These findings provided experimental basis for preventing and treating paraquat-induced pulmonary injury.

Bioinformatics analysis showed that PCA revealed distinct separation between paraquat and control groups, validating the acute paraquat poisoning model in mice. DESeq2 R package analysis showed significantly downregulated KLF4 expression in the paraquat group. ClusterProfiler R package-based KEGG enrichment analysis indicated DEGs significantly enriched in inflammation-related pathways (adjusted $p < 0.01$), including mitophagy, the Hippo signaling, and epithelial tight junctions. To screen potential KLF4 target genes, GeneCards database analysis showed that KLF4, KLF4, a Krüppel-like family transcription factor, regulated expression by binding CACCC sequences in target gene promoters. Human KLF4 gene is located on chromosome 9q31 [35], functioning in various physiological processes. KLF4 promoted tissue

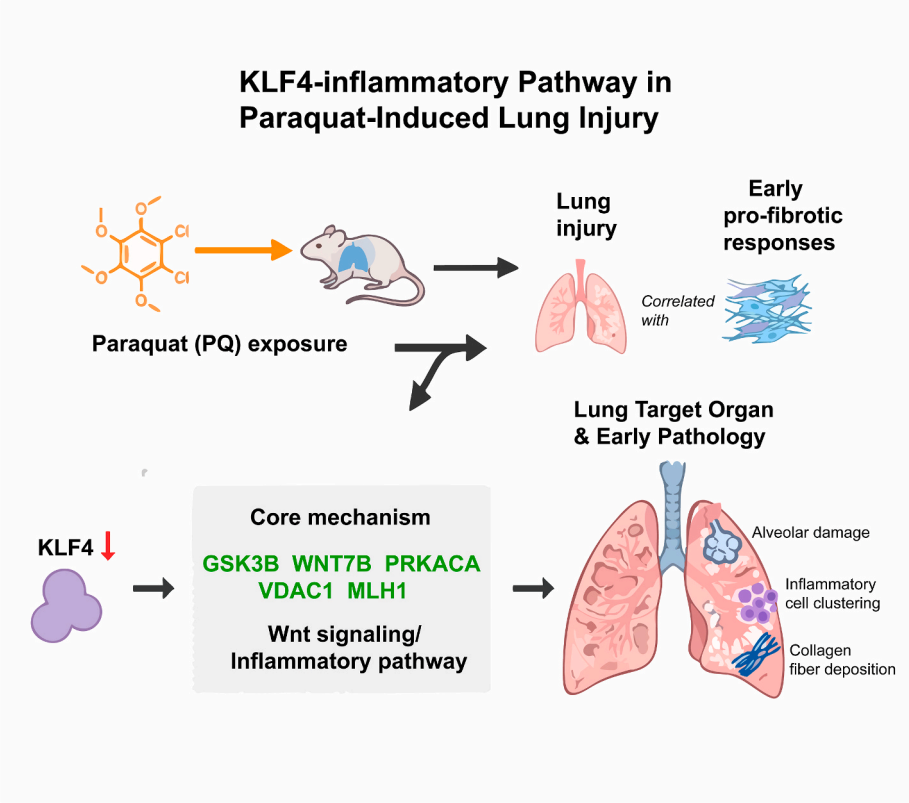

Fig. 5. The KLF4-inflammatory pathway is associated with paraquat-induced pulmonary injury and early pro-fibrotic responses.

development and homeostasis, critical for skin barrier development, and was involved in epithelial cell, bone, and kidney development [16]. It also regulated cell cycle by mediating p53-related pathways to participate in G1/S transition after DNA damage [36]. KLF4 alleviated inflammation and oxidative stress by inhibiting pro-inflammatory factors expression (NF-κB) and regulating antioxidant genes, to protect against oxidative damage [37]. In this study, pathway enrichment analysis of potential KLF4 target genes showed enrichment in inflammation-related pathways (Hippo signaling pathway and Wnt signaling pathway), suggesting KLF4 may regulate these pathways in inflammation. Based on this, we hypothesized that paraquat exposure correlated with KLF4 downregulation, which may link to the loss of potential transcriptional repression on downstream inflammation-related genes and the subsequent activation of pathways such as the Wnt signaling pathway, a change implicated in pulmonary tissue damage. To verify this, pathway topological analysis identified some core target genes (GSK3B, WNT7B and PRKACA), and key pathways (Wnt signaling pathway and cytokine response), with WNT7B showing significant negative correlation with KLF4 ($r = -0.9042$, $p = 0.002$). Paraquat poisoning was clinically challenging, with complex toxicity involving multiple pathway disorders [38]. The Wnt signaling pathway, regulating cell proliferation, differentiation, migration, and apoptosis, is divided into canonical Wnt/β-catenin and non-canonical pathways, with the former well-studied [39]. Study showed that paraquat dynamically regulated Wnt/β-catenin. In the acute phase, paraquat generated excessive reactive oxygen species (ROS) via redox cycling, inducing oxidative stress. High ROS oxidatively modified key molecules (β-catenin, GSK-3β) of the Wnt signaling pathway, activating GSK-3β to promote β-catenin degradation, and inhibiting Wnt signaling, exacerbating inflammation, apoptosis, and tissue damage finally [40]. In the chronic fibrotic phase, paraquat activated Wnt/β-catenin to promote EMT, fibroblast activation, and extracellular matrix deposition [41]. These findings suggest Wnt signaling pathway regulation as a potential strategy to alleviate paraquat toxicity, such as activating Wnt/β-catenin to enhance antioxidant and anti-apoptotic capacities [42], which made its regulatory mechanism critical for understanding toxicity and developing therapies. Box plots of core target genes (GSK3β, VDAC1, PRKACA, WNT7B) showed significant upregulation in the paraquat group ($p < 0.01$), with significant negative correlations with KLF4 expression. Combined with the known transcriptional repressor function of KLF4, the reduction of KLF4 in paraquat-exposed mice correlated with the upregulation of these core target genes and the subsequent activation of downstream pathways, a correlation that was consistent with the occurrence of pulmonary injury. VDAC1 (mitochondrial stress), a non-selective voltage-gated ion channel, mediates anion/cation transport across mitochondrial outer membrane and plasma membrane, binding signaling molecules (ceramides, phosphatidylcholines, cholesterol) [43]. PRKACA (inflammation amplification) encodes protein kinase A (PKA) catalytic subunit α, phosphorylating substrates in cytoplasm/nucleus to exert redox effects [44]. WNT7B (EMT driver) acts on Frizzled receptors, participating in canonical Wnt/β-catenin signaling [41]. Paraquat-induced KLF4 inactivation upregulated these core target genes, causing abnormal DNA repair, oxidative stress exacerbation, and inflammation-fibrosis transition.

There were some limitations and future directions for this study. First, the current study only demonstrates a significant correlative association between KLF4 downregulation and inflammatory pathway activation in paraquat-induced pulmonary injury, and no definitive causal relationship has been confirmed. Correlation analyses (Fig. 4D–E) support the potential role of KLF4, but functional validation with KLF4 overexpression/knockout mice is needed to confirm the causal relationship between KLF4 and the expression of core target genes/inflammatory markers. Second, the dynamic role of KLF4 in chronic pulmonary fibrosis is unclear. Therefore, further analysis extending the observation period to 14 days is vital to characterize KLF4's dynamic association with fibrosis markers. Third, screening for KLF4 agonists to test their therapeutic effects on paraquat-induced pulmonary injury will facilitate clinical translation, and future studies will also explore the specific

regulatory mechanism of KLF4 on the Wnt signaling pathway in pulmonary injury.

To summarize, this study corroborated that paraquat induced pulmonary injury and early pro-fibrotic responses, with the 30 mg/kg treatment group showing the most stable and significant phenotypic changes. Bioinformatics analysis identified KLF4 as a key gene and inflammation-related pathways as potential associated pathways, suggesting that paraquat-induced pulmonary injury and early pro-fibrotic responses were associated with KLF4 downregulation and subsequent activation of pathways such as the Wnt signaling pathway (Fig. 5).

Ethics statement

The animal study was reviewed and approved by the Laboratory Animal Welfare and Ethics Committee of Dongguan People's Hospital (Approval No.: IACUC-AWEC-202409500).

Funding statement

This work was supported by the Dongguan Science and Technology of Social Development Program [grant number 20231800940752]; the Medical Scientific Research Foundation of Guangdong Province, China [grant number B2023247]; the Natural Science Foundation of China [grant number 82470067]; the Initiation Project of Doctor Scientific research Fund of Dongguan People's Hospital [grant number K202301].

CRediT authorship contribution statement

Wei Zhang: Formal analysis, Methodology, Writing – original draft, Writing – review & editing. **Sisi Ye:** Formal analysis, Validation. **Jiabao Chen:** Data curation, Investigation. **Jingjing Cao:** Data curation, Resources. **Dongyang Xie:** Supervision. **Xiao Jin:** Funding acquisition. **Zhefan Xie:** Data curation, Formal analysis, Funding acquisition, Supervision. **Chunlai Fu:** Conceptualization, Funding acquisition, Methodology.

Declaration of competing interest

The authors declare that the research was conducted in the absence of any commercial or financial relationships that could be construed as potential conflicts of interest.

Acknowledgments

All authors make a significant contribution to the work reported, whether that is in the conception, study design, execution, acquisition of data, analysis and interpretation, or in all these areas; participated in drafting, revising or critically reviewing the article; have agreed on the journal to which the article has been submitted; and agree to be accountable for all aspects of the work.

We would like to express our sincere gratitude to Dr. Yi Li for her constructive comments during the manuscript revision, as well as the professional technical support in the design, preparation, and optimization of Graphic abstract, which greatly improved the clarity and presentation of this work.

Appendix A. Supplementary data

Supplementary data to this article can be found online at https://doi.org/10.1016/j.bbrep.2026.102648.

Data availability

All data generated in this work are presented as graphs and can be provided by the corresponding author upon reasonable request.

References

[1] T. Nazish, et al., Understanding paraquat resistance mechanisms in Arabidopsis thaliana to facilitate the development of paraquat-resistant crops, Plant Commun. 3 (3) (2022) 100321.
[2] J. Chen, et al., Effect of paraquat on cytotoxicity involved in oxidative stress and inflammatory reaction: a review of mechanisms and ecological implications, Ecotoxicol. Environ. Saf. 224 (2021) 112711.
[3] Y.T. Zhang, et al., [Epidemiological characteristics and toxicant type of acute poisoning cases in China, 2016-2022], Zhonghua Liuxingbingxue Zazhi 45 (10) (2024) 1376–1382.
[4] A. Samsidar, S. Siddiquee, S.M. Shaarani, A review of extraction, analytical and advanced methods for determination of pesticides in environment and foodstuffs, Trends Food Sci. Technol. 71 (2018) 188–201.
[5] R.K. Yadav, et al., Acute paraquat poisoning complicated by acute kidney injury and lung fibrosis: a case report from Nepal, Ann. Med. Surg. 85 (10) (2023) 5117–5119.
[6] X. Liu, H. Yang, Z. Liu, Signaling pathways involved in paraquat-induced pulmonary toxicity: molecular mechanisms and potential therapeutic drugs, Int. Immunopharmacol. 113 (Pt A) (2022) 109301.
[7] R. Subbiah, R.R. Tiwari, The herbicide paraquat-induced molecular mechanisms in the development of acute lung injury and lung fibrosis, Crit. Rev. Toxicol. 51 (1) (2021) 36–64.
[8] R.J. Dinis-Oliveira, et al., Paraquat poisonings: mechanisms of lung toxicity, clinical features, and treatment, Crit. Rev. Toxicol. 38 (1) (2008) 13–71.
[9] S. Dong, et al., A pqr2 mutant encodes a defective polyamine transporter and is negatively affected by ABA for paraquat resistance in Arabidopsis thaliana, J. Plant Res. 129 (5) (2016) 899–907.
[10] Y. Pu, et al., MANF inhibits NLRP3 inflammasome activation by competitively binding to DDX3X in paraquat-stimulated alveolar macrophages, Ecotoxicol. Environ. Saf. 287 (2024) 117331.
[11] Y. Zhao, et al., [CT manifestations and prognosis of acute paraquat induced lung injury], Zhonghua Lao Dong Wei Sheng Zhi Ye Bing Za Zhi 38 (2) (2020) 140–144.
[12] R.R. Chen, et al., A review for natural polysaccharides with anti-pulmonary fibrosis properties, which may benefit to patients infected by 2019-nCoV, Carbohydr. Polym. 247 (2020) 116740.
[13] Y. Lu, et al., 4-1BB signaling promotes alveolar macrophages-mediated pro-fibrotic responses and crystalline silica-induced pulmonary fibrosis in mice, Front. Immunol. 9 (2018) 1848.
[14] L. Huang, et al., Risk assessment based on dose-responsive and time-responsive genes to build PLS-DA models for exogenously induced lung injury, Ecotoxicol. Environ. Saf. 256 (2023) 114891.
[15] L. Leng, et al., Pathological features of COVID-19-associated lung injury: a preliminary proteomics report based on clinical samples, Signal Transduct. Targeted Ther. 5 (1) (2020) 240.
[16] Z. He, J. He, K. Xie, KLF4 transcription factor in tumorigenesis, Cell Death Discov. 9 (1) (2023) 118.
[17] G.D. Leikauf, et al., Integrative assessment of chlorine-induced acute lung injury in mice, Am. J. Respir. Cell Mol. Biol. 47 (2) (2012) 234–244.
[18] C.E. Cowan, et al., Kruppel-like factor-4 transcriptionally regulates VE-cadherin expression and endothelial barrier function, Circ. Res. 107 (8) (2010) 959–966.
[19] Y. Wang, et al., Peroxiredoxin 6 gene-targeted mice show increased lung injury with paraquat-induced oxidative stress, Antioxid Redox Signal 8 (1–2) (2006) 229–237.
[20] D. Zhang, et al., Tenascin-C participates pulmonary injury induced by paraquat through regulating TLR4 and TGF-beta signaling pathways, Inflammation 45 (1) (2022) 222–233.
[21] X. Yuan, et al., The effects of the combination of sodium ferulate and oxymatrine on lipopolysaccharide-induced acute lung injury in mice, Inflammation 35 (3) (2012) 1161–1168.
[22] K. Yu, et al., ATRA activates and PDGF-BB represses the SM22α promoter through KLF4 binding to, or dissociating from, its cis-DNA elements, Cardiovasc. Res. 90 (3) (2011) 464–474.
[23] O. Ilnytska, et al., Molecular mechanisms for activation of the agouti-related protein and stimulation of appetite, Diabetes 60 (1) (2011) 97–106.
[24] N. Adhikari, et al., Remarkable recovery in a patient with lethal dose paraquat poisoning: a case report, JNMA J Nepal Med Assoc 61 (265) (2023) 738–740.
[25] F. Yirmibes, E. Yalcin, K. Cavusoglu, Protective role of green tea against paraquat toxicity in Allium cepa L.: physiological, cytogenetic, biochemical, and anatomical assessment, Environ. Sci. Pollut. Res. Int. 29 (16) (2022) 23794–23805.
[26] E. Luis, et al., Altered expression of Thyroid- and calcium ion channels-related genes in rat testes by short-term exposure to commercial herbicides paraquat or 2,4-D, J Xenobiot 14 (4) (2024) 1450–1464.
[27] Y. Zhang, et al., The effects of Aquaporin-1 in pulmonary edema induced by fat embolism syndrome, Int. J. Mol. Sci. 17 (7) (2016).
[28] P.R. Gupta, Ambroxol hydrochloride in the management of idiopathic pulmonary fibrosis: clinical trials are the need of the hour, Lung India 31 (1) (2014) 43–46.
[29] S. Cui, et al., Ghrelin ameliorates A549 cell apoptosis caused by paraquat via p38-MAPK regulated mitochondrial apoptotic pathway, Toxicology 426 (2019) 152267.
[30] Z. Sun, et al., Paraquat induces pulmonary fibrosis through Wnt/beta-catenin signaling pathway and myofibroblast differentiation, Toxicol. Lett. 333 (2020) 170–183.
[31] W. Wu, Y. Li, Lung injury caused by paraquat poisoning results in increased interleukin-6 and decreased microRNA-146a levels, Exp. Ther. Med. 16 (1) (2018) 406–412.

[32] B. Hinz, et al., The myofibroblast: one function, multiple origins, Am. J. Pathol. 170 (6) (2007) 1807–1816.
[33] J.E. Eriksson, Cytoskeletal crosstalk in macrophages: vimentin drives ECM remodeling in tumor invasion and tissue plasticity, Dev. Cell 60 (12) (2025) 1655–1657.
[34] Y. Zhang, et al., Naringin mitigates paraquat-induced pulmonary epithelial-mesenchymal transition and fibrosis by modulating the NDRG1/JNK/PPARγ signaling pathway, Ecotoxicol. Environ. Saf. 302 (2025) 118542.
[35] S.K. Ray, The transcription regulator kruppel-like factor 4 and its dual roles of oncogene in glioblastoma and tumor suppressor in Neuroblastoma, For Immunopathol Dis Therap 7 (1–2) (2016) 127–139.
[36] H.S. Yoon, X. Chen, V.W. Yang, Kruppel-like factor 4 mediates p53-dependent G1/S cell cycle arrest in response to DNA damage, J. Biol. Chem. 278 (4) (2003) 2101–2105.
[37] Y. Liang, et al., A review of KLF4 and inflammatory disease: current status and future perspective, Pharmacol. Res. 207 (2024) 107345.
[38] X. Liu, H. Yang, Z. Liu, Signaling pathways involved in paraquat-induced pulmonary toxicity: molecular mechanisms and potential therapeutic drugs, Int. Immunopharmacol. 113 (Pt A) (2022) 109301.
[39] E.Y. Rim, H. Clevers, R. Nusse, The wnt pathway: from signaling mechanisms to synthetic modulators, Annu. Rev. Biochem. 91 (2022) 571–598.
[40] R. Nusse, H. Clevers, Wnt/beta-Catenin signaling, disease, and emerging therapeutic modalities, Cell 169 (6) (2017) 985–999.
[41] J. Liu, et al., Wnt/beta-catenin signalling: function, biological mechanisms, and therapeutic opportunities, Signal Transduct. Targeted Ther. 7 (1) (2022) 3.
[42] J. Wu, et al., Microtubule nucleation from the fibrous corona by LIC1-pericentrin promotes chromosome congression, Curr. Biol. 33 (5) (2023) 912–925.e6.
[43] T. Arif, A. Shteinfer-Kuzmine, V. Shoshan-Barmatz, Decoding cancer through silencing the mitochondrial gatekeeper VDAC1, Biomolecules 14 (10) (2024).
[44] R.E. Turnham, J.D. Scott, Protein kinase A catalytic subunit isoform PRKACA; history, function and physiology, Gene 577 (2) (2016) 101–108.